Layer-by-layer Multilayer Films Self-assembled from a Rare-earth-containing Poly-oxometalate $Na_9[Eu(W_5O_{18})_2]$ and Poly (allylamine hydrochloride) and Their Photoluminescent Properties

WANG, Yong-Hui[a](王永慧) WANG, Xin-Long[a](王新龙) HU, Chang-Wen*,[a](胡长文)
WANG, En-Bo[a](王恩波) SHI, Chun-Shan[b](石春山)

[a] *Institute of Polyoxometalate Chemistry, Faculty of Chemistry, Northeast Normal University, Changchun, Jilin 130024, China*

[b] *Changchun Institute of Applied Chemistry, Chinese Academy of Sciences, Changchun, Jilin 130022, China*

Ultrathin multilayer films of a rare-earth-containing polyoxometalate $Na_9[Eu(W_5O_{18})_2]$ (EW) and poly (allylamine hydrochloride) (PAH) have been prepared by layer-by-layer self-assembly from dilute aqueous solutions. The fabrication process of the EW/PAH multilayer films was followed by UV-vis spectroscopy and ellipsometry, which show that the deposition process is linear and highly reproducible from layer to layer. An average EW/PAH bilayer thickness of *ca*. 2.1 nm was determined by ellipsometry. In addition, the scanning electron microscopy (SEM) image of the EW/PAH film indicates that the film surface is relatively uniform and smooth. The photoluminescent properties of these films were also investigated by fluorescence spectroscopy.

Keywords layer-by-layer self-assembly, multilayer film, rare-earth-containing polyoxometalate, polyelectrolyte, photoluminescent property

Introduction

Recently, considerable interest has been devoted to assembling nanoscale building blocks with various inorganic and/or organic compositions into ultrathin multilayered films by versatile assembling strategies as these films can offer great potential for applications such as composites, catalysis, microelectronics, non-linear optics, sensors, and display technologies.[1-7] Several techniques such as Langmuir-Blodgett (LB) deposition,[8,9] sol-gel processing[10,11] and layer-by-layer (LbL) self-assembly[1,3,12-24] have been employed to produce these ordered assemblies. The layer-by-layer (LbL) self-assembly method, initially developed to prepare multilayer assemblies of polymers,[12-15] has been successfully applied to the fabrication of a variety of ordered composite films that incorporate organic components,[16-18] biopolymers and virus particles,[19-21] or inorganic materials such as clay[3] and nanoparticles.[22-24] This technique, based on the sequential adsorption of oppositely charged species from dilute solutions, is particularly attractive and has been proved to be a simple, yet powerful approach for constructing building blocks of different compositions into ultrathin multilayer films with controlled thickness and controlled molecular architecture at the nanometer level on essentially arbitrary solid substrates.[1] In addition, there are advantages in the low cost of instrumentation and high throughput of layer fabrication in comparison with LB deposition technique.

Polyoxometalates (POMs) are currently attracting much attention as building blocks for functional composite materials because of their particularly interesting nano-sized structure[25,26] and their potential applications in

* E-mail: huchw@nenu.edu.cn; Fax (Tel.): 0431-5640694

Received July 18, 2001; revised October 23, 2001; accepted November 11, 2001.
Project supported by the National Natural Science Foundation of China (No. 20071007) and the Foundation for University Key Teacher by the Ministry of Education of China.

catalysis, conductivity, photo- and electro-chromic devices and molecular electronics.[27-30] However, practical applications of POMs in these areas rely largely on the successful fabrication of thin POM-containing films.[31] So far, several reports[31-34] show that the LbL method is also adaptable for the preparation of thin nanocomposite films from a cationic polyelectrolyte and a negatively charged POM. The assembly process and adsorption mechanism have been studied in these publications while the properties of these films as materials are rarely reported.[32] Furthermore, to the best of our knowledge, no reports on the fabrication of LbL self-assembled films incorporating rare-earth-containing POMs or the properties of these films have been published up till now.

Here, we present the first fabrication of stable ultrathin composite films of a rare-earth-containing POM $Na_9[Eu(W_5O_{18})_2]$[35,36] (EW) and polyallylamine hydrochloride (PAH) by the LbL method. The film structure was characterized by UV-vis spectroscopy, ellipsometry and scanning electron microscopy (SEM). The fluorescent properties of these films have also been investigated by fluorescence spectroscopy.

Experimental

UV-vis spectra were recorded on a 756 CRT UV-visible spectrophotometer made in Shanghai, China. Ellipsometric measurements were performed with an AUEL-III Automated Laser Ellipsometer (Xi'an Jiaotong University, China, 2-mW HeNe laser, $\lambda = 632.8$ nm, angle of incidence 70° for silicon substrates). Thickness data were average values obtained from different spots (5—6) on a given sample and the error is ± 0.8 nm. Scanning electron micrograghs (SEM) were obtained on a Hitachi S-570 scanning electron microscope operating at 20 kV. Fluorescence spectra were obtained with an SPEX FL-2T2 fluorescence spectrophotometer. Further, solid substrates were cleaned by immersion in a solution containing 1 part NH_4OH (29 wt% aqueous solution), 1 part H_2O_2 (30 wt% aqueous solution), and 5 parts pure water at 70 ℃ for 20 min, followed by rinsing with copious amounts of deionized water.

The EW/PAH composite films were prepared by first depositing alternating poly(ethyleneimine) (PEI, MW 50000), poly(sodium 4-styrenesulfonate) (PSS, MW 70000), and poly(allylamine hydrochloride) (PAH, MW 70000) layers onto a cleaned substrate so as to form a PEI/PSS/PAH (P) precursor film. The solutions for the deposition of these polyelectrolyte layers were 10^{-2} mol/L PEI in water, 10^{-2} mol/L PSS in 1 mol/L NaCl, and 10^{-2} mol/L PAH in 1 mol/L NaCl (the polyelectrolyte concentration was based on the molecular weight of the monomer unit). The immersion time used was 20 min and the substrate was rinsed with deionized water and dried with nitrogen after each deposition step. The uppermost layer of PAH provides a positively-charged surface for subsequent self-assembly of an EW layer using the same immersion time and a concentration of 10^{-3} mol/L in water. Repeated cycles of PAH and EW deposition (with a final layer of PAH) result in multilayer structures of the form $P/(EW/PAH)_n$.

Results and discussion

UV-vis spectroscopy has been proved to be a useful and facile technique to evaluate the growth process of multilayers[31-34] and was thus used in the present work to monitor the LbL assembling process of EW/PAH films. Fig. 1 shows the UV-vis absorption spectra of $(EW/PAH)_n$ multilayers (with $n = 7$) assembled on a precursor PEI/PSS/PAH film on a quartz substrate. As shown in Fig. 1, these films exhibit the characteristic bands of EW at 195 nm and 260 nm pertaining to the oxygen to tungsten charge transfer transitions,[37] substantiating the incorporation of the EW polyanions into the composite film without any alteration. The feature band at 225 nm is due to the benzene chromophores in PSS,[31,34] while PAH does not absorb above 200 nm.[31] Since the f→f bands of Eu^{3+} in the visible region are very weak,[37] the UV-vis spectra of the EW/PAH films do not show these bands. As shown in the inset of Fig. 1, the absorbances of quartz-supported $P/(EW/PAH)_n$ multilayer films at two characteristic wavelengths (195 nm and 260 nm) increase proportionally with the number of adsorption cycles, n. This nearly linear growth of the absorption peaks indicates that approximately equal amounts of EW and PAH were deposited for each adsorption procedure and that the EW/PAH films have grown uniformly with each deposition cycle.

Further evidence for uniform multilayer growth of EW/PAH assemblies is obtained from optical ellipsometry measurements. As shown in Fig. 2, ellipsometry of the $P/(EW/PAH)_{13}$ film assembled on a single-crystal silicon substrate indicates a linear increase in the thickness of the

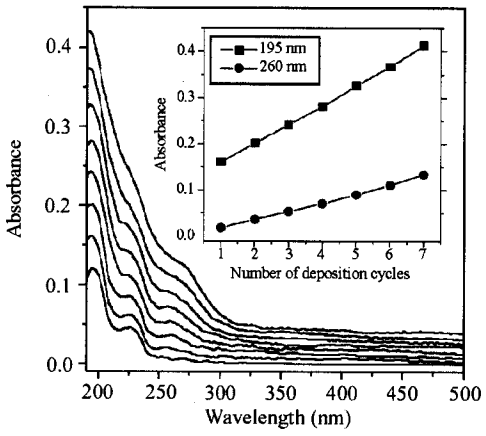

Fig. 1 UV-vis absorption spectra of $(EW/PAH)_n$ multilayer films with $n = 0$—7 on a PEI/PSS/PAH-modified quartz substrate. The lowest curve corresponds to the precursor film ($n = 0$). The other curves, from bottom to top, correspond to $n = 1$, 2, 3, 4, 5, 6 and 7, respectively. The inset shows plots of the absorbance values at 195 nm and 260 nm as a function of the number of deposition cycles (n).

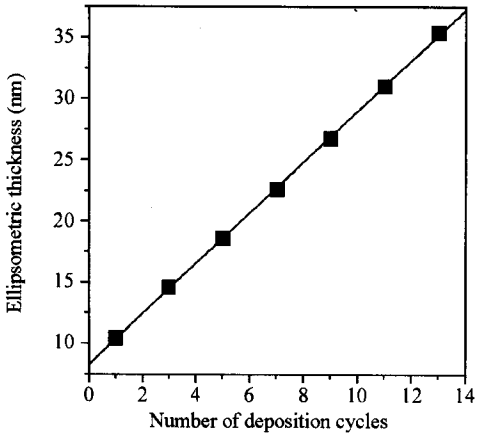

Fig. 2 Ellipsometric thickness of a multilayered structure on a single-crystal silicon substrate as a function of the number of deposition cycles (n) for 13 complete EW/PAH cycles, in which the straight line represents the linear fit of the data. All data in this figure were averages over five points on one sample.

multilayered structure with the number of deposition cycles. This clearly demonstrates that deposition is very reproducible and film growth is essentially uniform, that is, in each adsorption cycle equivalent amounts of EW and PAH are deposited on the substrates. From ellipsometry the average film thickness for the EW/PAH bilayer is determined to be *ca*. 2.1 nm. This value is consistent with the monolayer thickness of EW based on its cluster diameter of *ca*. 0.8 nm in the short axis[38] and the 1.2-nm film thickness for a single PAH layer.[34] The schematic representation of the internal film structure is shown in Fig. 3. In addition, ellipsometric measurements also establish a thickness of ~ 8.2 nm for the precursor PEI/PSS/PAH film.

Although UV-vis absorption spectroscopy and ellipsometry confirmed the uniform growth of the EW/PAH multilayer assemblies via electrostatic LbL adsorption, these techniques can only characterize the film homogeneity on the macroscopic scale. Scanning electron microscopy (SEM) can provide further detailed information involving the surface morphology and the homogeneity of the LbL films down to the nanometer scale. Fig. 4 shows the SEM image of a $P/(EW/PAH)_{10}$ multilayer film prepared on a silicon wafer. It can be seen that the film surface is relatively smooth over a large area. However, this SEM image also shows some individual domains. This perhaps arises from the adsorption of bi- and multi-layer aggregates of the EW polyanions and/or the PAH polyelectrolyte chains.

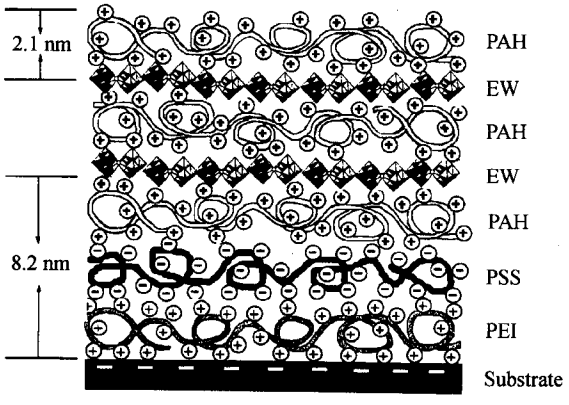

Fig. 3 Schematic representation of the internal layer structure of a PEI/PSS/PAH/$(EW/PAH)_2$ multilayer film self-assembled on a substrate. Note that this drawing is an oversimplification of the actual layer structure.

Fig. 5 (a) shows the photoluminescence spectrum of a solid sample of EW and Fig. 5 (b) shows that of the $P/(EW/PAH)_8$ films self-assembled on a smooth quartz substrate excited at room temperature, respectively. When $[Eu(W_5O_{18})_2]^{9-}$ is excited in the intense UV bands corresponding to the oxygen-tungsten transitions within the $[Eu(W_5O_{18})_2]^{9-}$ "ligand" or in the weak visible bands corresponding to f - f excited states of the Eu^{3+}

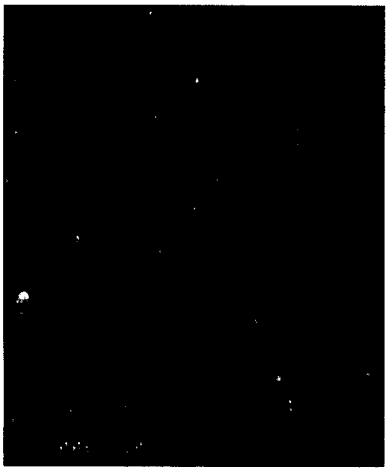

Fig. 4 Scanning electron micrograph of a P/(EW/PAH)$_{10}$ multilayer on a silicon wafer (surface view). The sample was prepared at 20-min adsorption of EW and PAH (ten cycles) on a PEI/PSS/PEI precursor film.

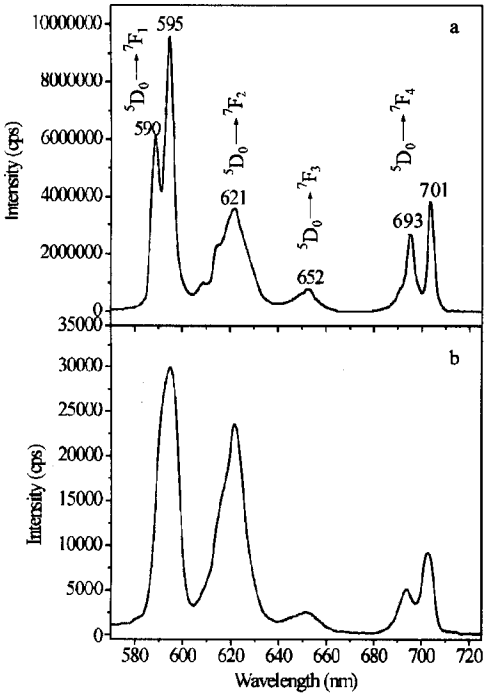

Fig. 5 Photoluminescence spectra of a solid sample of EW (a) and a P/(EW/PAH)$_8$ multilayer films assembled on a quartz substrate (b), both excited in the UV region at room temperature.

ion in the visible region at room temperature, weak luminescence arising from the $^5D_0 \rightarrow {}^7F_J$ ($J = 0$—4) transitions can be observed.[39] As shown in Fig. 5, for the EW/PAH film, the photoluminescence spectrum exhibits multiple peak structure, very similar to that found for the EW solid. This again confirms that the structure of [Eu$(W_5O_{18})_2$]$^{9-}$ is retained after incorporation into the film, that is, the [Eu$(W_5O_{18})_2$]$^{9-}$ polyanions can exist in the film stably. As shown in Fig. 5 (a), the most intense bands at *ca*. 590 nm and 595 nm correspond to the $^5D_0 \rightarrow {}^7F_1$ emission transition. The broad band around 621 nm is also relatively intense and ascribed to the $^5D_0 \rightarrow {}^7F_2$ emission transition. The less intense bands at 693 nm and 701 nm are assigned to the $^5D_0 \rightarrow {}^7F_4$ emission transition, while the very small band at *ca*. 652 nm corresponds to the $^5D_0 \rightarrow {}^7F_3$ emission transition.[37-39] However, the $^5D_0 \rightarrow {}^7F_0$ emission transition at *ca*. 580 nm, which can hardly be identified at room temperature or under low resolution,[37] is practically absent in both spectra. This Eu^{3+} emission pattern for the EW solid corresponds to the C_{4v} site symmetry of Eu^{3+}.[38] Further, it is noteworthy that for Fig. 5 (a) and (b) there are some variations in the relative intensity, multiplicity and width of individual bands. Above all, the $^5D_0 \rightarrow {}^7F_1$ and $^5D_0 \rightarrow {}^7F_2$ emission transitions, which are respectively split into a doublet and an approximate triplet in the spectrum of the EW solid, are not split in the spectrum of the LbL film. This may be associated with the relatively low content and uniform distribution of EW in the LbL film, and most of all, the strong electrostatic interaction between the EW polyanions and the PAH polycations, which probably induces the variation in symmetry and strength of the molecular electric field surrounding the Eu^{3+} ion and the modification of the interaction of the Eu^{3+} ion with its environment.[40,41] Since it is generally believed that the less symmetrical the geometric arrangement surrounding the rare-earth ion, the more numerous the lines appearing in the spectrum due to internal Stark splitting of the "unperturbed" ionic levels,[40] the disappearance of the splitting of the $^5D_0 \rightarrow {}^7F_1$ and $^5D_0 \rightarrow {}^7F_2$ emission transitions in the present case may be attributed to the higher symmetry of the molecular field around Eu^{3+} ion in the film than that in the solid (C_{4v}). In the second place, it is also noteworthy that the $^5D_0 \rightarrow {}^7F_2$ emission transition becomes more intense for the film than for the solid. This can be explained by the fact that this transition is hypersensitive and its transition probability can increase considerably by minor changes in the surroundings.[37] On the whole, the changes in the molecular electric field of the Eu^{3+} ion determine the important variations in relative intensity, width and splitting of the individual emission bands.[40]

Conclusions

A simple but powerful strategy based on LbL self-assembly has been used for preparing stable ultrathin mutilayer films that incorporate a rare-earth-containing POM. The films have displayed a linear increase in the absorption and film thickness with the number of deposition cycles. SEM image indicates that the films are relatively uniform and smooth. The photoluminescent properties of the multilayer film are similar to those observed for the solid of the rare-earth-containing POM, which is of potential importance to the fabrication of photoluminescent thin film materials incorporating POMs. This method may be adaptable to other POMs and the study on this respect is still underway.

References and notes

1 Decher, G. *Science* **1997**, *277*, 1232.
2 Greenham, N. C.; Moratti, S. C.; Bradeley, D. D. C.; Friend, R. H.; Holmes, A. B. *Nature* **1993**, *365*, 628.
3 Kleinfeld, E. R.; Ferguson, G. S. *Science* **1994**, *265*, 370.
4 Katz, H. E.; Schiling, M. L. *Chem. Mater.* **1993**, *5*, 1162.
5 Gao, G.; Hong, H.-G.; Mallouk, T. E. *Acc. Chem. Res.* **1992**, *25*, 420.
6 Fendler, J. H.; Meldrum, F. C. *Adv. Mater.* **1995**, *7*, 607.
7 Maoz, R.; Yam, R.; Sagiv, J. In *Organic Thin Films and Surfaces: Directions for the Ninneties*, Ed.; Ulman, A., Academic Press, San Diego, **1995**, p. 41.
8 Blodgett, K. B.; Langmuir, I. *Phys. Rev.* **1937**, *51*, 964.
9 Ulman, A. *An Introduction to Ultrathin Organic Films: From Langmuir-Blodgett to Self-Assembly*, Academic Press, Boston MA, **1991**.
10 Ichinose, I.; Senzu, H.; Kunitake, T. *Chem. Lett.* **1996**, 831.
11 Fan, H.; Zhou, Y.; Lopez, G. P. *Adv. Mater.* **1997**, *9*, 728.
12 Decher, G.; Hong, J. D. *Makromol. Chem., Makromol. Symp.* **1991**, *46*, 321.
13 Decher, G.; Hong, J. D.; Schmitt, J. *Thin Solid Films* **1992**, *210/211*, 831.
14 Fou, A. C.; Rubner, M. F. *Macromolecules* **1995**, *28*, 7115.
15 Caruso, F.; Niikura, K.; Furlong, D. N.; Okahata, Y. *Langmuir* **1997**, *13*, 3422.
16 Watanabe, S.; Regen, S. L. *J. Am. Chem. Soc.* **1994**, *116*, 8855.
17 Zhang, X.; Shen, J. *Adv. Mater.* **1999**, *11*, 1139.
18 Sun, J.; Wu, T.; Liu, F.; Wang, Z.; Zhang, X.; Shen, J. *Langmuir* **2000**, *16*, 4620.
19 Lvov, Y.; Decher, G.; Sukhorukov, G. *Macromolecules* **1993**, *26*, 5396.
20 Lvov, Y.; Ariga, K.; Ichinose, I.; Kunitake, T. *J. Am. Chem. Soc.* **1995**, *117*, 6117.
21 Lvov, Y.; Haas, H.; Decher, G.; Möhwald, H. *Langmuir* **1994**, *10*, 4232.
22 Schmitt, J.; Decher, G.; Geer, R. E.; Shashidhar, R.; Calvert, J. M. *Adv. Mater.* **1997**, *9*, 61.
23 Hao, E.; Lian, T. *Langmuir* **2000**, *16*, 7879.
24 Wu, T.; Zhang, X. *Chem. J. Chin. Univ.* **2001**, *22*, 1057 (in Chinese).
25 Zhang, S.; Huang, G.; Shao, M.; Tang, Y. J. *Chem. Soc., Chem. Commun.* **1993**, 37.
26 Müller, A.; Krickemeyer, E.; Dillinger, S.; Bögge, H.; Plass, W.; Proust, A.; Dloczik, L.; Menke, C.; Meyer, J.; Rohlfing, R. *Z. Anorg. Allg. Chem.* **1994**, *620*, 599.
27 For a recent overview on polyoxometalate chemistry refer to *Chem. Rev.* **1998**, *98*, 1 and references therein.
28 Hu, C.; He, Q.; Zhang, Y.; Liu, Y.; Tang, T.; Zhang, J. *Chem. Commun.* **1996**, 121.
29 Guo, Y.; Wang, Y.; Hu, C.; Wang, Y.; Wang, E. *Chem. Mater.* **2000**, *12*, 3501.
30 Guo, Y.; Li, D.; Hu, C.; Wang, Y.; Wang, E.; Zhou, Y.; Feng, S. *Appl. Catal. B* **2001**, *30*, 337.
31 Caruso, F.; Kurth, D. G.; Volkmer, D.; Koop, M. J.; Müller, A. *Langmuir* **1998**, *14*, 3462.
32 Moriguchi, I.; Fendler, J. H. *Chem. Mater.* **1998**, *10*, 2205.
33 Ichinose, I.; Tagawa, H.; Mizuki, S.; Lvov, Y.; Kunitake, T. *Langmuir* **1998**, *14*, 187.
34 Kurth, D. G.; Volkmer, D.; Ruttorf, M.; Richter, B.; Müller, A. *Chem. Mater.* **2000**, *12*, 2829.
35 Peacock, R. D.; Weakley, T. J. R. *J. Chem. Soc. A* **1971**, 1836.
36 EW was prepared as described by Peacock and Weakley (see Ref. 35) with the composition $Na_9[Eu(W_5O_{18})_2]\cdot \sim 18H_2O$.
37 Ballardini, R.; Mulazzani, Q. G.; Venturi, M.; Bolletta, F.; Balzani, V. *Inorg. Chem.* **1984**, *23*, 300.
38 Sugeta, M.; Yamase, T. *Bull. Chem. Soc. Jpn.* **1993**, *66*, 444.
39 Blasse, G.; Dirksen, G. J.; Zonnevijllle, F. *J. Inorg. Nucl. Chem.* **1981**, *43*, 2847.
40 Filipescu, N.; Sager, W. F.; Serafin, F. A. *J. Phys. Chem.* **1964**, *68*, 3224.
41 Cunha, M. C. F.; Brito, H. F.; Zinner, L. B.; Vicentini, G. *Coord. Chem. Rev.* **1992**, *119*, 1.

(E0107181 SONG, J. P.; HUANG, W. Q.)